Supported Tantalum Oxide Catalysts: Synthesis, Physical Characterization, and Methanol Oxidation Chemical Probe Reaction

Yongsheng Chen,[†] Jose L. G. Fierro,[‡] Tsunehiro Tanaka,[§] and Israel E. Wachs*[,†]

In Situ Molecular Characterization & Catalysis Laboratory, Department of Chemical Engineering, Lehigh University, Bethlehem, Pennsylvania 18015, Instituto de Catalisis y Petroleoquimica, CSIC, Cantoblanco, 28049 Madrid, Spain, and Department of Molecular Engineering, Graduate School of Engineering, Kyoto University, Kyoto, 606-8501, Japan

Received: December 6, 2002; In Final Form: March 27, 2003

Supported tantalum oxide catalysts on Al_2O_3, TiO_2, ZrO_2, and SiO_2 supports were prepared by the incipient wetness impregnation method. The catalysts were characterized by X-ray photoelectron spectroscopy (XPS), Raman spectroscopy, and X-ray absorption near edge structure (XANES) under hydrated and dehydrated conditions. The Al_2O_3-, TiO_2-, and ZrO_2-supported tantalum oxide catalysts possess similar surface TaO_x molecular structures, consisting primarily of polymerized surface TaO_5/TaO_6 species at high surface coverage. The surface Ta atom density at monolayer coverage are also similar and were found to be 4.5, 6.6, and 6.3 Ta atoms/nm^2 on the Al_2O_3, TiO_2, and ZrO_2 supports, respectively. The SiO_2-supported tantalum oxide catalyst is very different and consists of isolated TaO_4 species with a much lower maximum surface Ta density, 0.7 Ta atoms/nm^2, due to the lower concentration and reactivity of the silica hydroxyls. The catalytic properties of the surface TaO_x species were chemically probed with the methanol oxidation reaction. The Al_2O_3-, TiO_2-, and ZrO_2-supported tantalum oxide catalysts, possessing monolayer surface coverage of surface TaO_x species, were found to exhibit 100% dimethyl ether originating from surface acidic sites. The TOF_{acidic} values varied by almost 2 orders of magnitude, reflecting the influence of the specific oxide support on the surface TaO_x acidic sites through the bridging Ta−O−support bond. In contrast, the surface TaO_x species on SiO_2 were found to possess redox characteristics rather than acidic characteristics. Thus, the specific reactivity and selectivity of the surface TaO_x species strongly depend on the specific oxide support ligand and its effect on the bridging Ta−O−support bond.

Introduction

The group 5 (V, Nb, and Ta) metal oxide catalysts, both as bulk and supported metal oxides, have received much attention in recent years.[1−7] Vanadia catalysts are employed in many industrial processes, such as selective oxidation of hydrocarbons to chemical intermediates and the selective catalytic reduction of NO_x with NH_3. Fundamental understanding of the surface vanadia molecular structures and their relationships with the catalytic reaction mechanisms have been achieved in recent years.[1−3] Comparative studies have also been carried out on bulk and supported niobia catalysts and much is currently known about the molecular structure−reactivity/selectivity relationships of niobia-based catalysts.[3−7] In contrast, the current fundamental understanding of tantala-based catalytic materials is rather limited.[3,4]

However, quite a few applications of supported tantalum oxide catalysts have been reported in recent years. For example, supported Ta_2O_5/SiO_2 is found to be useful for vapor-phase decomposition of methyl *tert*-butyl ether (MTBE) to isobutene and methanol,[8] vapor-phase Beckmann rearrangement of cyclohexanone oxime to caprolactam,[8] and as a photoactive catalyst for the oxidation of CO to CO_2 and ethanol to diethyl acetal;[9] supported Ta_2O_5/Al_2O_3 catalyzes liquid-phase oxidation of unsaturated fatty acids and hydrocarbon cracking;[10,11] and supported Ta_2O_5/TiO_2 is able to synthesize methanethiol (CH_3-SH) from mixtures of H_2S and CO.[12]

There are two investigations in the literature about the molecular structures of the surface tantalum oxide species. An in situ X-ray absorption near edge structure (XANES) study of SiO_2-supported tantalum oxide found that the dehydrated surface TaO_x species possesses TaO_4 coordination with a single terminal Ta═O bond.[9] UV−vis DRS and FT-Raman studies similarly concluded that for dehydrated SiO_2-supported tantalum oxide, surface TaO_4 species exists at low tantalum oxide coverage, whereas surface TaO_6 species also appears at high surface coverage due to the presence of $Ta_2O_5 \cdot nH_2O$ microcrystals.[13] The UV−vis DRS and FT-Raman investigations also concluded that both dehydrated surface TaO_4 and TaO_6 species exist on Al_2O_3 and ZrO_2 supports at all surface coverages. Furthermore, the surface tantalum oxide species were found to possess a higher number of Lewis acidic sites than those of the corresponding surface vanadia species.

In this paper, supported tantalum oxide catalysts on four different oxide supports (Al_2O_3, SiO_2, TiO_2, and ZrO_2) were prepared via the incipient wetness impregnation of tantalum ethoxide and physically characterized with different physical characterization techniques (XPS, Raman, and XANES) under hydrated and dehydrated conditions. The catalytic properties of the surface TaO_x species were chemically probed with the methanol oxidation reaction, and the relationship between the surface TaO_x molecular structure and the activity/selectivity was investigated. In addition, an empirical relationship between Ta−O bond length and the Raman frequency shifts was

* To whom correspondence should be addressed. E-mail: iew0@lehigh.edu.
[†] Lehigh University.
[‡] Instituto de Catalisis y Petroleoquimica.
[§] Kyoto University.

10.1021/jp0276451 CCC: $25.00 © 2003 American Chemical Society
Published on Web 05/09/2003

developed and applied to predict the bond length of Ta−O bonds with different bond order. The surface Ta density of polymerized species was further predicted.

Experimental Section

1. Catalyst Preparation. The oxide supports used for this study were Al_2O_3 (Engelhard, $S_{BET} = 222$ m^2/g), SiO_2 (Cabosil EH-5, $S_{BET} = 332$ m^2/g), TiO_2 (Degussa P-25, $S_{BET} = 55$ m^2/g), and ZrO_2 (Degussa, $S_{BET} = 39$ m^2/g). The supported tantalum oxide catalysts were prepared by the incipient wetness impregnation method with a tantalum ethoxide precursor (H. C. Starck, 99.99%). The supports were impregnated with ethanol solutions of tantalum ethoxide and dried at room temperature under flowing N_2 in a glovebox. After they were transferred to a furnace, the samples were initially heated to 120 °C for 2 h under flowing dry air and then calcined at 500 °C for 5 h. Bulk Ta_2O_5(L) ($S_{BET} = 4$ m^2/g) and tantalum oxyhydrate, $Ta_2O_5 \cdot nH_2O$ ($S_{BET} = 69$ m^2/g), were also obtained from H. C. Starck. The $Ta_2O_5 \cdot nH_2O$ was further calcined at 500 °C for 2 h, which resulted in a BET surface area of 23 m^2/g.

2. Catalyst Characterization. *2.1. X-ray Photoelectron Spectroscopy (XPS).* XPS spectra were collected with a Fisons ESCALAB 200R electron spectrometer equipped with a hemispherical electron analyzer and a Mg Kα X-ray source ($h\nu =$ 1253.6 eV) powered at 120 W. A PDP 11/05 computer from DEC was used for collecting and analyzing the spectra. The samples were placed in small copper cylinders and mounted on a transfer rod placed in the pretreatment chamber of the instrument. All samples were outgassed at 500 °C to remove adsorbed moisture before the XPS analysis. The binding energies (BE) were referenced to Si 2p at 103.4 eV with an accuracy of 0.2 eV. The Ta $4f^{7/2}$, Al 2p, Ti $2p^{3/2}$, Si 2p, and Zr $3d^{5/2}$ electron intensities were also used for quantitative analysis. The atomic concentration ratios were calculated by correcting the intensity ratios with the theoretical sensitivity factors proposed by the manufacturer.

2.2. Raman Spectroscopy. Raman spectra were obtained with the 514.5 nm line of an Ar^+ ion laser (Spectra Physics, model 164). The exciting laser power was measured at the sample to be about 10−50 mW. The scattered radiation from the sample passed through a SPEX triple-mate monochromator (model 1877) and detected by an OMA III (Princeton Applied Research, model 1463) optical multichannel analyzer with a photodiode array cooled thermoelectrically to −35 °C. The catalyst samples were pressed into self-supporting wafers. The hydrated samples were rotated at 2000 rpm to minimize local heating and to avoid dehydration by the laser beam. The Raman spectra of the dehydrated samples were recorded at room temperature and were obtained after heating the sample in flowing O_2 at 400−450 °C for 1 h in a stationary quartz cell, which has been previously described.[14]

2.3. X-ray Absorption Near Edge Structure (XANES). XANES analysis was performed with the XAFS (X-ray absorption fine structure) spectrometer installed on the BL01B1 beam line13 with a Si(111) two-crystal monochromator at SPring-8 at the Japan Synchrotron Radiation Research Institute (JASRI) located at Hyogo, Japan. Before the XANES measurement, the dehydrated samples were heated to 673 K in vacuo, treated under a 60 Torr oxygen atmosphere, pressed into a disk under dry nitrogen, and sealed with a polypropylene film. The hydrated samples were kept at high humidity >90% at room temperature for more than 10 days. Details of the data processing are described elsewhere.[15]

3. Catalysis. The methanol oxidation reaction was carried out in a fixed-bed differential reactor operating at atmospheric pressure. A mixture of helium and oxygen from two mass flow controllers (Brooks 5850) was bubbled through a methanol saturator cooled by flowing water from a cooler (Neslab RTE 110) to obtain a 6/13/81 (mol %) mixture of methanol/oxygen/helium at a flow rate of ∼100 sccm. The reactor was vertically held and made of 6-mm o.d. Pyrex glass, and the flow direction was downward. The catalysts were placed at the middle of the tube between two layers of quartz wool and about 20−70 mg of catalysts was used depending on the catalyst reactivity. Before the methanol oxidation reaction, the catalysts were pretreated at 400 °C for 30 min with flowing oxygen and helium in order to remove adsorbed moisture and any carbonaceous residues. The outlet line of the reactor to the GC was heated to ∼120−140 °C to avoid condensation of methanol and its products. The reaction products were analyzed by an online GC (HP 5840) equipped with TCD and FID detectors, and two separation columns (Carboxene-1000 packed column and CP-sil 5CB capillary column) connected in parallel. By increasing the temperature of the catalyst bed, the reaction would initiate at some point with a detectable amount of products and the temperature was subsequently raised by ∼10 °C until the total conversion of methanol reached ∼10%. For each supported tantalum oxide catalyst, the conversion/selectivity as a function of temperature was measured and the Arrhenius activation energy was also determined. Furthermore, the turnover frequency ($TOF_{overall}$), the number of methanol molecules converted per surface TaO_x species per second, was also calculated since below monolayer coverage of the surface TaO_x species the tantalum oxide dispersion would be 100%.

Results

1. X-ray Photoelectron Spectroscopy (XPS). XPS was employed in this work to determine the monolayer surface coverages of tantalum oxide on the different oxide supports. The XPS atomic ratios of Ta to the different support cations are presented in Figure 1 as a function of the loading of Ta_2O_5. As a common observation, the ratio initially increases linearly with the tantalum oxide loading and then deviates from the linear relationship with a significantly reduced slope at a certain loading. The "break" in the curve is due to the transition from 2D surface TaO_x species to the 3D microcrystals, with the latter having a low XPS sensitivity.[16] Two straight lines can be drawn, as shown in the figures, and their intercept determines monolayer surface coverage. The monolayer values for Al_2O_3, TiO_2, ZrO_2, and SiO_2 supports were determined to be ∼24%, ∼11%, ∼8%, and ∼12% Ta_2O_5, respectively. These values correspond to maximum surface densities of 4.5, 6.6, 6.3, and 0.7 Ta atoms/nm^2 for tantalum oxide supported on Al_2O_3, TiO_2, ZrO_2, and SiO_2, respectively.

2. XANES. For the Ta L1-edge, the energy resolution is intrinsically poor due to the broad bandwidth of the L1 (2s) level ($\Delta E = 5.58$ eV full width at half-maximum). Therefore, preedge peaks appear broad and it is not possible to determine the TaO_x surface molecular structure on the basis of peak positions (the shift of which is thought to be less than 2 eV). The preedge peak area (integrated intensity), however, can be used to determine the molecular structure. The preedge peak was extracted by subtracting the background, which was created by fitting a fourth-order polynomial to the XANES spectrum in the 20−23 and 38−40 eV regions as shown in Figure 2. The peak area was calculated by the Simpson method. TaO_4 structures have different peak area values than TaO_6 or TaO_5 structures. The TaO_4 structures possess values greater than 0.7, and the TaO_6/TaO_5 structures possess values less than 0.5.[9] The

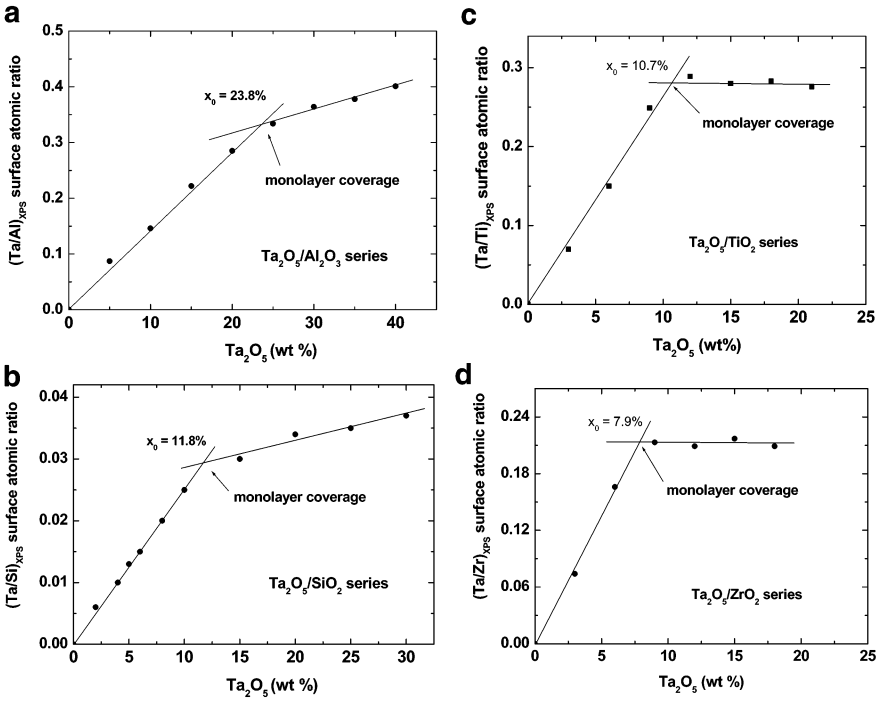

Figure 1. The XPS surface atomic ratio of Ta/support cation vs Ta_2O_5 loading for the supported tantalum oxide catalysts, (a) Ta_2O_5/Al_2O_3, (b) Ta_2O_5/SiO_2, (c) Ta_2O_5/TiO_2, and (d) Ta_2O_5/ZrO_2.

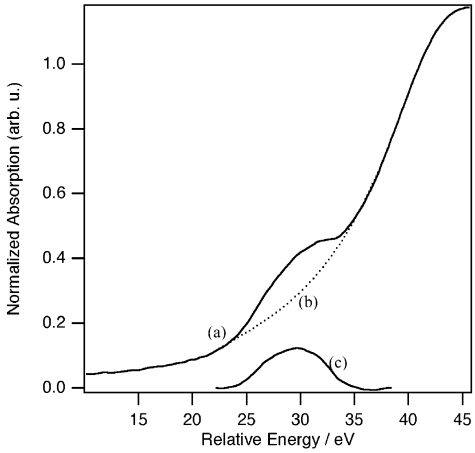

Figure 2. Determination of the XANES preedge areas and the Ta coordination, (a) original spectrum, (b) fourth-order polynomial background, and (c) background subtracted spectrum.

TABLE 1: XANES Results of Ta Coordination of Surface TaO_x Species on Different Oxide Supports under Hydrated and Dehydrated Conditions

	hydrated		dehydrated	
catalyst	area	coordination	area	coordination
Ta_2O_5/Al_2O_3	0.57	TaO_6/TaO_5	0.50	TaO_6/TaO_5
Ta_2O_5/SiO_2	0.44	TaO_6/TaO_5	0.77	TaO_4
Ta_2O_5/TiO_2	0.44	TaO_6/TaO_5	0.48	TaO_6/TaO_5
Ta_2O_5/ZrO_2	0.46	TaO_6/TaO_5	0.46	TaO_6/TaO_5

peak area values between 0.5 and 0.7 correspond to mixture of TaO_6/TaO_5 and a small amount of TaO_4. The XANES results are presented in Table 1. Essentially all the hydrated supported tantalum oxide catalysts possess TaO_6/TaO_5 coordination and the hydrated Ta_2O_5/Al_2O_3 also contains a small amount of some TaO_4 species. For the dehydrated supported tantalum oxide catalysts, TaO_6/TaO_5 is the dominant coordination with the exception of Ta_2O_5/SiO_2, which only possesses a TaO_4 coordination.

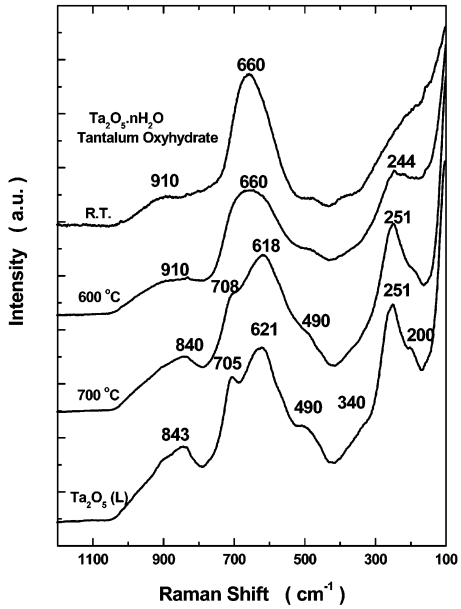

Figure 3. Raman spectra of bulk Ta_2O_5 and tantalum oxyhydrate before and after different heat treatments.

3. Raman Spectroscopy. The Raman spectra of bulk tantalum oxyhydrate, $Ta_2O_5 \cdot nH_2O$, before and after exposure to elevated temperatures in air for 2 h are presented in Figure 3. For comparison, the spectrum of the low-temperature phase of crystalline Ta_2O_5(L) is also presented in Figure 3. Tantalum oxyhydrate is amorphous with a major characteristic broad Raman band at ~660 cm^{-1} due to Ta−O vibration. The heat treatment at 600 °C does not affect the main Raman bands of tantalum oxyhydrate, but a new band begins to emerge at ~244 cm^{-1}. However, further heat treatment at 700 °C transforms the amorphous tantalum oxyhydrate phase into well crystallized Ta_2O_5(L) structure. The Raman results are in agreement with previous thermogravimetric analysis (TGA) and XRD studies of tantalum oxyhydrate by González and co-workers,[17] which concluded that at 600 °C the tantalum oxyhydrate lost little water

and remained amorphous and that at 800 °C and above most of the water of hydration was lost and the tantalum oxyhydrate crystallized into different bulk structures of tantalum oxide (at least two phases with a reversible phase transition occurring at about 1360 °C).[18] The strongest Ta_2O_5(L) band appears at ~100 cm^{-1} and the second strongest at ~251 cm^{-1}. The characteristic broad band at ~660 cm^{-1} for the amorphous tantalum hydrate splits into at least two peaks at 621 and 705 cm^{-1} when it crystallizes to Ta_2O_5(L). Other weak Raman bands are also observed at approximately 200, 340, 490, and 843 cm^{-1} and can be assigned as follows: L-Ta_2O_5 lattice photon at 100 cm^{-1}; 340 cm^{-1} due to TaO_6 symmetric bending; Ta−O symmetric stretching at 621 cm^{-1}; higher order of Ta−O symmetric stretching at 843 cm^{-1}; and bridging Ta−O−Ta bending, symmetric, and antisymmetric stretching vibrations at 251, 490, and 705 cm^{-1}, respectively.

The main features of the Raman spectra of the hydrated Ta_2O_5/Al_2O_3 catalysts change at loadings between 20% and 25% Ta_2O_5 as shown in Figure 4a. Below 20% Ta_2O_5/Al_2O_3, there is only a single major Raman band at ~910 cm^{-1}. For 25% Ta_2O_5/Al_2O_3 and higher loadings, another Raman band appears at ~660 cm^{-1} and its relative intensity to that of ~910 cm^{-1} band increases with the increasing tantalum oxide loading. Thus, bulk tantalum oxyhydrate formed above monolayer coverage of surface TaO_x (Raman band at 660 cm^{-1}) and the hydrated surface TaO_x species exhibits one main Raman band at ~910 cm^{-1}. Monolayer coverage of the surface TaO_x on Al_2O_3 occurs between 20% and 25% Ta_2O_5/Al_2O_3 because bulk tantalum oxyhydrate begins to form in this region. The supported bulk $Ta_2O_5 \cdot nH_2O$ phase is more difficult to crystallize during elevated heat treatment than unsupported pure $Ta_2O_5 \cdot nH_2O$ since Raman spectroscopy reveals that even up to 800 °C the main features of the spectra remain without the appearance of the bands characteristic of crystalline Ta_2O_5(L).

The main Raman features of the surface TaO_x species on Al_2O_3 change significantly upon dehydration (compare parts a and b of Figure 4). There are three main Raman bands for the dehydrated surface TaO_x species at ~940, ~740, and ~610 cm^{-1}. The Raman band at ~940 cm^{-1} corresponds to the symmetric stretching mode of the dehydrated terminal Ta═O bond, and the bands at ~740 and ~610 cm^{-1} are assigned to the antisymmetric and symmetric stretching modes of the dehydrated bridging Ta−O−Ta bond, respectively. The presence of bridging Ta−O−Ta bands for dehydrated Ta_2O_5/Al_2O_3 reveals that polymerized surface TaO_x species is present on the Al_2O_3 surface. The weak band at ~400 cm^{-1} is assigned to the bending mode of the dehydrated surface TaO_x species. "Ghost peaks" due to strong Raleigh scattering are observed for Al_2O_3- and SiO_2-supported Ta_2O_5 catalysts; the physical "filtering" of the spectra below Raman shift of ~250 cm^{-1} avoids the effect; hence, only the region above 300 cm^{-1} is presented.

The Raman spectra of the hydrated Ta_2O_5/SiO_2 catalysts are presented in Figure 5. Similar to the hydrated Ta_2O_5/Al_2O_3 catalysts, the hydrated surface TaO_x species exhibit a Raman band at 940 cm^{-1}, seen as a weaker shoulder on the Si−OH vibration at ~975 cm^{-1}, and the bulk tantalum oxyhydrate phase displays a band at 685 cm^{-1} (the apparent shift from 660 to 685 cm^{-1} of this phase is most likely due to the strong background of the SiO_2 vibrations in this region). The Raman signals for the Ta_2O_5/Al_2O_3 catalysts are much stronger than those of the Ta_2O_5/SiO_2 because of the higher concentration of surface TaO_x species, and with the presence of relatively strong background SiO_2 vibrations, the band positions of the latter are not as well resolved. The Raman band of the bulk tantalum

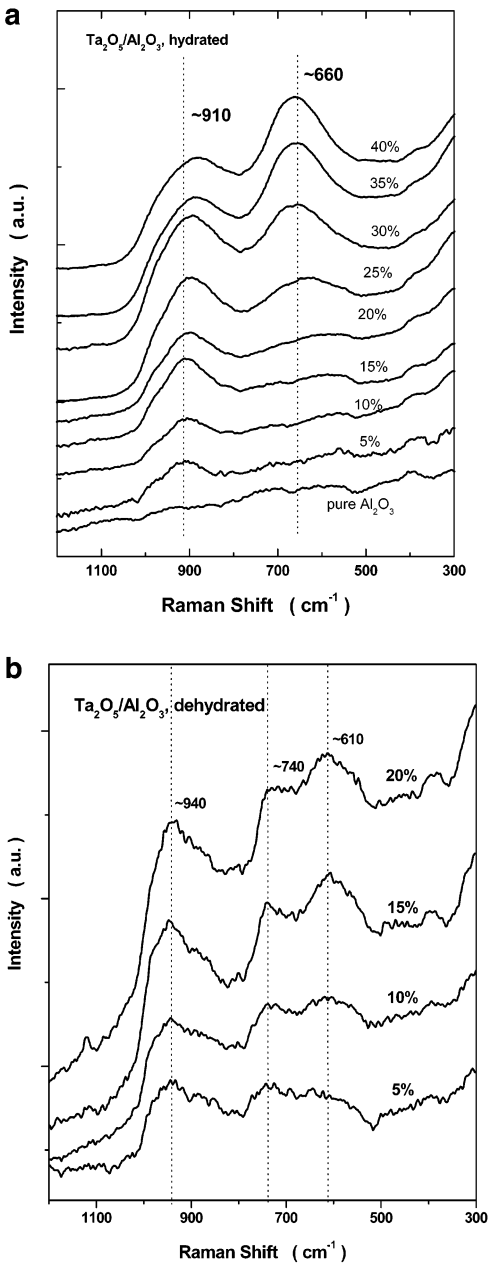

Figure 4. Raman spectra of supported Ta_2O_5/Al_2O_3 oxide catalysts: (a) hydrated and (b) dehydrated.

oxyhydrate phase at ~685 cm^{-1} appears for 6% Ta_2O_5/SiO_2 and higher tantalum oxide loadings, suggesting that maximum coverage of surface TaO_x on SiO_2 occurs between 4% and 6% Ta_2O_5/SiO_2. Dehydration of the supported Ta_2O_5/SiO_2 catalysts does not significantly alter the features of the hydrated Ta_2O_5/SiO_2 Raman spectra (not shown) because of the relatively weak surface tantalum oxide signals and the much stronger bands due to the SiO_2 support in the same region.

The TiO_2 and ZrO_2 supports give rise to very strong Raman bands below 800 cm^{-1}, and thus, only Raman bands above 800 cm^{-1} can be detected for the TiO_2- and ZrO_2-supported tantalum oxide catalysts, as shown in Figures 6 and 7. Compared to the Raman bands of the surface TaO_x species, the strong oxide support bands at ~790 cm^{-1} for TiO_2 and ~756 cm^{-1} for ZrO_2 dominate the spectra. For the dehydrated 9% Ta_2O_5/TiO_2 sample, there is only some indication of the existence of vibrations from a surface tantalum oxide species at ~980, ~940, and ~855 cm^{-1}, after subtraction of the TiO_2 background, but

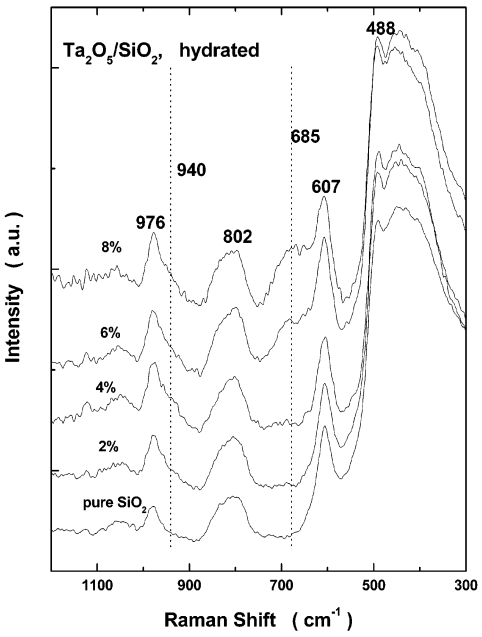

Figure 5. Raman spectra of hydrated Ta_2O_5/SiO_2 catalysts.

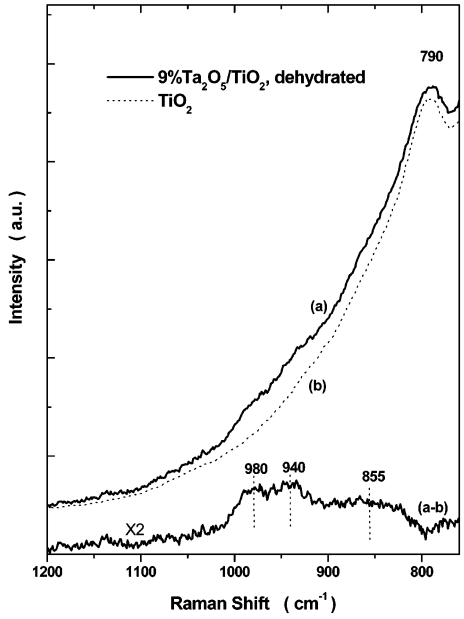

Figure 6. Raman spectra of (a) dehydrated 9% Ta_2O_5/TiO_2 catalyst and (b) TiO_2 support; spectrum c is the difference spectrum between (a) and (b).

the surface TaO_x bands are so weak and broad that these band positions are just a rough estimate. The Raman bands in the 940−980 cm^{-1} region are associated with a terminal Ta═O bond, and the 855 cm^{-1} band is consistent with the antisymmetric stretch of bridging Ta−O−Ta bonds. For the dehydrated 6% Ta_2O_5/ZrO_2 sample, the surface TaO_x bands are only slightly better resolved in Figure 7. Two broad Raman bands, at ∼976 and 932 cm^{-1}, after subtraction of the ZrO_2 background, corresponding to the terminal Ta═O bond. The bands at ∼822 and ∼725 cm^{-1} are assigned to antisymmetric stretching modes of the bridging Ta−O−Ta bonds. Thus, polymerized surface TaO_x species appear to be present on the TiO_2 and ZrO_2 supports. The hydrated Raman spectra of the Ta_2O_5/TiO_2 and Ta_2O_5/ZrO_2 catalysts did not give rise to apparent Raman bands of the surface TaO_x species because hydration results in even broader Raman bands.

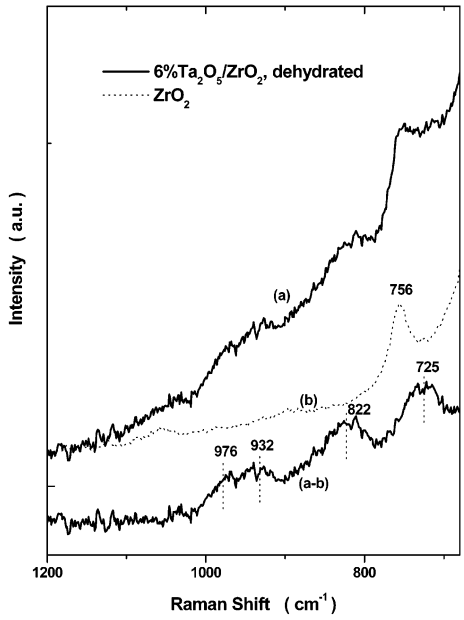

Figure 7. Raman spectra of (a) dehydrated 6% Ta_2O_5/ZrO_2 catalyst and (b) ZrO_2 support; spectrum c is the difference spectrum between (a) and (b).

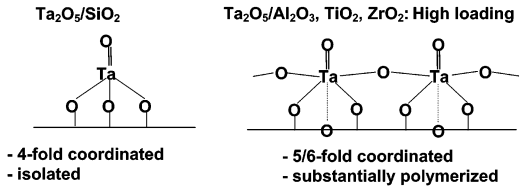

Figure 8. Schematic drawings of molecular structures of surface TaO_x species under dehydrated condition.

4. Methanol Oxidation. The methanol oxidation reaction chemically probes the nature of the catalyst surface sites via its reaction products: dimethyl ether (DME) results from surface acidic sites, formaldehyde (HCHO), methyl formate (MF), and dimethoxy methane (DMM) originate from surface redox sites and CO/CO_2 are produced on surface basic sites.[19] Bulk Ta_2O_5-(L) and $Ta_2O_5 \cdot nH_2O$ are solid acid catalysts, and the catalytic data for CH_3OH oxidation are in agreement with this conclusion since only DME is formed. The methanol oxidation selectivities and activities of the different supported tantalum oxide catalysts as well as those of the bulk Ta_2O_5(L), $Ta_2O_5 \cdot nH_2O$, and the pure oxide supports are presented in Table 2. The supported surface TaO_x monolayers on Al_2O_3, TiO_2, and ZrO_2 also possess 100% acidic surface sites since essentially only DME is formed during methanol oxidation. A significant portion of CO_x was observed for the lower tantalum oxide loaded Ta_2O_5/ZrO_2 catalysts due to the exposure of the surface zirconia sites below monolayer coverage, ∼8% Ta_2O_5/ZrO_2. For low Ta_2O_5/TiO_2 loadings, the exposed surface titania sites produced traces of HCHO byproducts below monolayer coverage, ∼11% Ta_2O_5/TiO_2. The selectivity of the SiO_2-supported tantalum oxide depends on the Ta_2O_5/SiO_2 loading. At low Ta_2O_5/SiO_2 loadings, the redox product HCHO and the basic product CO_2 are formed. The Ta_2O_5/SiO_2 appears to contain both surface redox and basic sites since SiO_2 is not catalytically active at this reaction temperature. At 5% Ta_2O_5/SiO_2 and higher tantalum oxide loadings, the main product is MF from surface redox sites, and the minor DME originates from the presence of surface acidic sites present on the bulk $Ta_2O_5 \cdot nH_2O$ phase.

The catalytic activities are expressed as the number of moles of methanol converted per hour per gram of catalyst and are

TABLE 2: Selectivity and Activity of Supported Tantalum Oxide Catalysts during CH_3OH Oxidation

(a) Supported Ta_2O_5/Al_2O_3 at 200 °C

catalyst	selectivity (%) DME	CO_x	DMM	activity (10^{-2} mol/g h)
Ta_2O_5(L)	100			0.072
Al_2O_3	100			13.3
2% Ta_2O_5/Al_2O_3	100			9.2
5% Ta_2O_5/Al_2O_3	100			8.6
10% Ta_2O_5/Al_2O_3	100			6.2
15% Ta_2O_5/Al_2O_3	100			4.5
20% Ta_2O_5/Al_2O_3	100			4.1
25% Ta_2O_5/Al_2O_3	100			2.9
30% Ta_2O_5/Al_2O_3	100			2.8
35% Ta_2O_5/Al_2O_3	100			2.3
40% Ta_2O_5/Al_2O_3	100			2.1

(b) Supported Ta_2O_5/SiO_2 at 300 °C

catalyst	selectivity (%) HCHO	CO_2	MF	DME	activity (10^{-2} mol/g h)
SiO_2					not active
2% Ta_2O_5/SiO_2	74	26			6.0
4% Ta_2O_5/SiO_2	66	34			17.4
5% Ta_2O_5/SiO_2			100	trace	6.3
6% Ta_2O_5/SiO_2			95	5	6.5
8% Ta_2O_5/SiO_2			84	16	6.7

(c) Supported Ta_2O_5/TiO_2 at 300 °C

catalyst	selectivity (%) DME	CO_x	HCHO	activity (10^{-2} mol/g h)
TiO_2	100		trace	0.34
3% Ta_2O_5/TiO_2	100		trace	0.42
6% Ta_2O_5/TiO_2	100		trace	0.47
9% Ta_2O_5/TiO_2	100		trace	0.56
12% Ta_2O_5/TiO_2	100			0.62
15% Ta_2O_5/TiO_2	100			1.09
18% Ta_2O_5/TiO_2	100			1.14

(d) Supported Ta_2O_5/ZrO_2 at 300 °C

catalyst	selectivity (%) DME	CO_x	HCHO	activity (10^{-2} mol/g h)
ZrO_2	trace	100		0.32
3% Ta_2O_5/ZrO_2	69	31		0.72
6% Ta_2O_5/ZrO_2	92	8		0.93
9% Ta_2O_5/ZrO_2	100			1.16
12% Ta_2O_5/ZrO_2	100			1.18
15% Ta_2O_5/ZrO_2	100			1.61
18% Ta_2O_5/ZrO_2	100			1.48

presented in Table 2. The activities of Ta_2O_5/Al_2O_3 catalysts continuously decrease with Ta_2O_5 loading, which suggests that the surface TaO_x acidic species on Al_2O_3 is less active than the surface acidic sites of the Al_2O_3 support but more active than the bulk $Ta_2O_5 \cdot nH_2O$ phase (possessing a relatively small number of exposed surface tantalum oxide sites). In contrast, the activities of the supported Ta_2O_5/TiO_2 and Ta_2O_5/ZrO_2 catalysts change with tantalum oxide loading: increasing up to monolayer coverage and continuing to increase after monolayer coverage. This activity pattern suggests that the surface TaO_x species on TiO_2 and ZrO_2 is more active than the corresponding oxide supports but less active than the bulk $Ta_2O_5 \cdot nH_2O$ phase. The selectivity of the supported Ta_2O_5/SiO_2 catalysts dramatically changes with tantalum oxide loading due to the varying nature of the surface tantala sites with surface coverage (See Raman section above).

Arrhenius relationships were obtained for CH_3OH oxidation over the supported tantalum oxide catalysts as well as the pure oxides and the apparent activation are presented in Table 3. Pure Ta_2O_5(L) and $Ta_2O_5 \cdot nH_2O$ possess the lowest activation energies of 13.7 and 15.0 kcal/mol, respectively. The acidic Al_2O_3 and TiO_2 supports exhibit a slightly higher activation energy of ~20 kcal/mol, and the basic ZrO_2 support exhibits a higher value of ~36 kcal/mol. The SiO_2 support was found to be inactive for CH_3OH oxidation in this temperature range and no activation energy could be determined. The acidic supported tantalum oxide species, yielding only DME, possess an activation energy of ~16−19 kcal/mol, which is intermediate between the acidic supports and bulk Ta_2O_5(L) and $Ta_2O_5 \cdot nH_2O$. Supported Ta_2O_5/SiO_2 exhibits a lower activation energy, but this is for the production of MF and cannot be compared to the acidic surface sites found in the other catalysts. The apparent activation energy E_{app} is an overall parameter describing the catalytic processes over the catalysts and is related to $E_{act} + \Delta H$, where ΔH is a negative value and the exothermic heat of adsorption of methanol. Nevertheless, E_{app} allows extrapolation of the methanol oxidation activities of the catalysts to nearby temperatures (especially for the very active Ta_2O_5/Al_2O_3 system, which required lower temperatures to ensure differential reaction conditions).

TABLE 3: Activation Energies of Supported Tantalum Oxide Catalysts at Monolayer Surface Coverage and Pure Bulk Oxides for CH_3OH Oxidation

catalyst	temperature range	activation energy (kcal/mol)	reaction products
Ta_2O_5(L)	220−260	13.7	DME
$Ta_2O_5 \cdot nH_2O$ (500 °C)	200−260	15.0	DME
Al_2O_3	150−190	20.2	DME
SiO_2	200−350		not active
TiO_2	300−350	19.8	DME
ZrO_2	300−350	36.4	CO_x
Ta_2O_5/Al_2O_3	170−210	18.6	DME
Ta_2O_5/TiO_2	290−340	16.3	DME
Ta_2O_5/ZrO_2	270−330	17.7	DME
Ta_2O_5/SiO_2	280−330	13.2	MF

Discussion

1. Surface TaO_x Density at Monolayer Coverage. The monolayer loadings of the surface TaO_x species on the different oxide supports were determined from the XPS measurements to be 23.8% Ta_2O_5/Al_2O_3, 10.7% Ta_2O_5/TiO_2, and 7.9% Ta_2O_5/ZrO_2. Raman reveals that the bulk $Ta_2O_5 \cdot nH_2O$ phase starts to appear on the Al_2O_3 support between 20% and 25% Ta_2O_5/Al_2O_3 (see Figure 4a). Raman is not able to detect the incipient formation of bulk $Ta_2O_5 \cdot nH_2O$ on the TiO_2 and ZrO_2 supports due to the strong Raman vibrations of the supports below 800 cm^{-1}, which overshadows the characteristic band of the bulk $Ta_2O_5 \cdot nH_2O$ phase at ~660 cm^{-1}. However, the methanol oxidation reaction provides information about the completion of the surface TaO_x monolayers on the oxide supports since exposed support sites give rise to side reactions (see Table 2). The TiO_2 support gives rise to trace amounts of HCHO, which disappears above 12% Ta_2O_5/TiO_2. The ZrO_2 support is very active in oxidizing methanol to CO_x, but CO_x is not detected above 9% Ta_2O_5/ZrO_2. These results suggest that the monolayer loading is between 9%−12% Ta_2O_5/TiO_2 and between 6%−9% Ta_2O_5/ZrO_2, which is in agreement with the XPS measurement results. Thus, for tantalum oxide supported on Al_2O_3, TiO_2, and ZrO_2, the monolayer surface coverage determined by XPS, Raman, and CH_3OH oxidation are in agreement.

For supported Ta_2O_5/SiO_2 catalysts, Raman reveals that the bulk of $Ta_2O_5 \cdot nH_2O$ phase already exists in the catalysts with loadings of 6% Ta_2O_5/SiO_2 and above (see Figure 5), whereas XPS suggests a monolayer coverage of 11.8% Ta_2O_5/SiO_2. The methanol oxidation reaction reveals that the reaction selectivity changes dramatically at a loading of 5% Ta_2O_5/SiO_2 (see Table

TABLE 4: Surface Ta Densities at Monolayer Surface Coverage on Different Oxide Supports

	BET surface area (m^2/g)			
support	original	tantalum oxide monolayer coverage	XPS monolayer loading (wt %)	Ta surface density (Ta/nm^2)
Al_2O_3	222	190	23.8	4.5
SiO_2	332	210	11.8 (5.0[a])	(0.7[a])
TiO_2	55	49	10.7	6.6
ZrO_2	39	37	7.9	6.3

[a] From Raman and methanol oxidation.

2), which is in agreement with the Raman results. The XPS measurement most probably resulted in a higher value for monolayer surface coverage for the Ta_2O_5/SiO_2 catalyst system because the weak interaction between SiO_2 and the surface TaO_x species resulted in an exterior surface composition, line-of-sight, that may not have been representative of the entire sample. In contrast, both Raman and the methanol oxidation probe the entire sample and are not limited to only the line-of-sight external composition. Thus, monolayer loadings of surface TaO_x on the different oxide supports correspond to 23.8% Ta_2O_5/Al_2O_3, 10.7% Ta_2O_5/TiO_2, 7.9% Ta_2O_5/ZrO_2, and 5.0% Ta_2O_5/SiO_2, respectively.

A BET measurement of the supported Ta_2O_5 catalysts near monolayer coverage shows shrinkage of the oxide supports after impregnation and calcination. The BET surface areas of 25% Ta_2O_5/Al_2O_3, 12% Ta_2O_5/TiO_2, 6% Ta_2O_5/ZrO_2, and 5% Ta_2O_5/SiO_2 are 143, 43, 35, and 200 m^2/g, respectively, so the surface areas of the supports at monolayer coverage are 190, 49, 37, and 210 m^2/g, accordingly. Thus, the surface densities of Ta atoms at monolayer coverage on the different oxide supports can be determined and are listed in Table 4. The monolayer surface TaO_x densities are 4.5, 6.6, 6.3, and 0.7 Ta atoms/nm^2 on Al_2O_3, TiO_2, ZrO_2, and SiO_2 supports, respectively.

Additional estimates of monolayer surface TaO_x coverage can also be determined from knowledge of the structures of surface TaO_x phases. Hardcastle and Wachs developed an empirical relationship between the Nb−O bond length and its stretching frequency,[20] referred to as the diatomic approximation,

$$\nu(\mathrm{Nb{-}O}) = 26262\mathrm{e}^{-1.9238R} \quad (1)$$

where ν is the stretching frequency (cm^{-1}) and R is the length of the Nb−O bond (Å). Due to the known similarity between Ta−O and Nb−O bonds,[21] a similar relationship can be derived for Ta−O by correcting the above expression with the higher mass of Ta, which results in

$$\nu(\mathrm{Ta{-}O}) = 25308\mathrm{e}^{-1.9238R} \quad (2)$$

Brown and Wu also presented a relationship between the bond valence s and bond length R for Ta−O:[21]

$$s(\mathrm{Ta{-}O}) = \left(\frac{R}{1.907}\right)^{-5} \quad (3)$$

For supported Ta_2O_5/Al_2O_3 catalysts under dehydrated conditions, the largest Raman shift observed for the terminal Ta═O bond of surface tantalum oxide species is ∼940 cm^{-1}, corresponding to a bond length of 1.71 Å and a bond valence of 1.72 from eqs 2 and 3, respectively.

The monolayer surface TaO_x density for the polymerized surface TaO_x species can be estimated from eq 3. A simplified structural model is proposed: the surface TaO_x species are identical with a "double bond" of valence 1.72. For a surface TaO_x unit to occupy the maximum area, a square pyramidal structure is assumed, which means that there are four bridging Ta−O bonds to the oxide support or adjacent surface TaO_x sites with each bond having valence of 0.82, which, from eq 3, corresponds to a Ta−O bond length of 1.98 Å. For bridging Ta−O−Ta bonds with an angle of 180°, a maximum distance between Ta atoms of 3.97 Å is obtained. Hence, the maximum area that a polymerized surface TaO_x unit can occupy is 15.8 $Å^2$ and its reciprocal gives the minimum surface Ta density of a monolayer of polymerized surface TaO_x species, 6.3 Ta atoms/nm^2. This value matches the experimental monolayer surface densities for Ta_2O_5/TiO_2 and Ta_2O_5/ZrO_2. The slightly lower surface TaO_x density on Al_2O_3 may be due to the presence of a minor amount of isolated surface TaO_4 units, which is detected by the XANES measurements.

TABLE 5: Methanol Oxidation Turnover Frequency (TOF) Values at 300 °C for Supported Tantalum Oxide Catalysts at Monolayer Coverage and Bulk Ta_2O_5

	TOF (10^{-3} s^{-1})	
catalyst	DME (acidic)	MF (redox)
Ta_2O_5(L)[a]	90	
Ta_2O_5/Al_2O_3	246	
Ta_2O_5/TiO_2	3.3	
Ta_2O_5/ZrO_2	8.4	
Ta_2O_5/SiO_2		78

[a] From ref 28.

2. Molecular Structures of the Surface TaO_x Species. Under hydrated conditions, the surfaces of the supported tantalum oxide catalysts possess a thin film of moisture and the aqueous solution chemistry controls the hydrated surface TaO_x species, which is determined by the pH value of the aqueous film and the concentration of TaO_x.[22] The oxide support influences the final pH value at the PZC theory (point of zero charge). The Al_2O_3, TiO_2, ZrO_2, and SiO_2 supports have net pH at PZC of 8.9, ∼6.2, ∼6.0, and 3.9, respectively. The presence of the acidic surface TaO_x overlayer will further lower the net pH at PZC since the Ta_2O_5 possesses a net pH at PZC of 2.9.[22,23] According to the hydrolysis of cations,[24] the Ta(V) species may form hexanuclear or mononuclear species at different pH values. The $Ta_6O_{19}^{6-}$(aq) species exists in very basic solutions and exhibits major Raman bands at ∼857 and ∼516 cm^{-1}.[25] The $Ta(OH)_5$ species exists at pH values between 1 and 12. Therefore, $Ta(OH)_5$ is the main hydrated TaO_x species on all the four oxide supports under hydrated conditions, and it exhibits its strongest Raman band at ∼910 cm^{-1} (see Figure 4). Under dehydrated conditions, the surface TaO_x species react with the surface hydroxyls of the oxide support and become anchored on the support. The extent of linkage among the surface species depends on a spatial factor: the distance between Ta atoms from each other and a chemical factor—the strength of the Ta atoms interacting with the oxide supports. The stronger the interaction, the less likely for the neighboring Ta species to form bridging bonds. Hence, scarce surface hydroxyls and strong interaction are favorable to the formation of isolated surface TaO_x species, while dense surface hydroxyls and weak interactions would be expected to favor the formation of polymerized surface TaO_x species. The surface Ta density at monolayer coverage is a reflection of the availability and reactivity of surface hydroxyls (see Table 4) and silica has less reactive surface hydroxyls than the other three supports.[26] H_2-TPR studies of supported vanadia catalysts[27] demonstrated that the strength of V−O−support band decreases in the order of SiO_2 > Al_2O_3 > ZrO_2 ∼ TiO_2 and that a similar trend could also be

TABLE 6: Acidic and Redox TOFs of Pure and Supported Tantalum Oxide and Niobium Oxide Catalysts[29] Containing Monolayer Surface Coverage during CH_3OH Oxidation at 230 °C

	acidic TOF ($\times 10^{-3}$ S^{1-})		redox TOF ($\times 10^{-3}$ S^{1-})	
oxide support	Ta_2O_5	Nb_2O_5	Ta_2O_5	Nb_2O_5
bulk	16.9	21	0	0
Al_2O_3	25.3	200	0	0
ZrO_2	0.97	50	0	0
TiO_2	0.45	40	0	0
SiO_2	0	0	15.6	62

expected for surface TaO_x species. Thus, the silica support possesses a lower concentration of reactive surface hydroxyls and a very strong interaction with the surface TaO_x species. Consequently, isolated species are most likely formed. For the other oxide supports, the polymerized surface TaO_x species are more favorable because of the higher concentration of reactive surface hydroxyls and somewhat weaker Ta−O-support interaction. This model is supported by the Raman and XANES data (see Table 1 and Figure 4). Under dehydrated conditions, surface TaO_x species on SiO_2 are isolated TaO_4 structures and surface TaO_x species on Al_2O_3, TiO_2, and ZrO_2 are present as polymerized surface TaO_5/TaO_6 structures as shown schematically in Figure 8. The TaO_4 unit has one Ta═O double and three Ta−O−Si bonds. The TaO_5/TaO_6 unit has two bridging Ta−O−Ta bonds and two bridging Ta−O−support bonds on Al_2O_3, TiO_2, and ZrO_2. For the surface TaO_6 structure, there could be another Ta−O−support bond at a much longer Ta−O bond length, which corresponds to an oxygen atom of the oxide support. The distribution of the number of surface TaO_x units in the polymerized surface TaO_x species is not known at present.

3. Structure Reactivity/Selectivity. The catalytic activities are expressed as the number of moles of methanol converted per hour per gram of catalyst and the TOF values are determined by normalizing the activities of the supported tantalum oxide catalysts at monolayer surface coverage to the number of surface TaO_x sites, which is the proper parameter to compare the activity of the surface active sites in different catalysts. TOF values were not determined below monolayer surface coverage since the exposed oxide supports are also active, with the exception of SiO_2. The activities of the supported Ta_2O_5 catalysts at monolayer surface coverage were determined from a linear interpolation of the activities of two nearest loading catalysts (slightly below and above monolayer coverage). The TOF values of the monolayer-supported TaO_x species at 300 °C are presented in Table 5. The TOF values of the different supported tantalum oxide catalysts vary by almost 2 orders of magnitude, which reveals a significant infuence of the specific oxide support via the bridging Ta−O−support bond. The acidic surface sites on bulk Ta_2O_5(L) are less active than the surface TaO_x species on Al_2O_3 but are significantly more active than the acidic sites on the other supported tantalum oxides. Furthermore, the supported surface TaO_x species is 100% dispersed, whereas only a very small fraction of surface TaO_x sites of the bulk Ta_2O_5 are accessible (low dispersion). Thus, the total activity for supported tantalum oxide catalysts can be higher than that of the bulk Ta_2O_5 with the same number of Ta atoms (see Table 2). The corresponding supported niobia catalysts have the same coordination as the supported tantala catalysts and the TOF_{acidic} values of the supported niobia catalysts are significantly greater than that of their supported tantala analogues as shown in Table 6. Furthermore, the H_2-TPR of Ta_2O_5/Al_2O_3 shows almost no reduction up to 700 °C, suggesting that surface TaO_x species is stable during methanol oxidation and retains the same molecular structure as the dehydrated surface TaO_x species.[30]

Conclusions

The molecular structures and catalytic properties of supported tantalum oxide catalysts depend on the specific oxide support. The Al_2O_3-, TiO_2-, and ZrO_2-supported tantalum oxide catalysts consist of polymerized surface TaO_5/TaO_6 species under dehydrated conditions with very similar surface TaO_x densities at monolayer surface coverage and possess 100% acidic sites. The TOF values vary by almost 2 orders of magnitude revealing a significant influence of the oxide support through the bridging Ta−O−support bond (Al ≫ Zr > Ti). The dehydrated SiO_2-supported tantalum oxide catalyst only consists of isolated surface TaO_4 species, before formation of $Ta_2O_5 \cdot nH_2O$ microcrystals, with a much lower surface TaO_x density at maximum coverage and possesses mostly redox properties. The specific oxide support is proposed to be the major factor that determines the molecular structure, TOF, and selectivity of the supported surface TaO_x species.

Acknowledgment. The financial support of H.C. Starck for this research is gratefully acknowledged.

References and Notes

(1) *Appl. Catal. A* **1997**, *157* (special issue devoted to vanadium oxide compounds).
(2) Wachs, I. E.; Weckhuysen, B. M. *Appl. Catal. A* **1997**, *157*, 67.
(3) Wachs, I. E.; Briand, L. E.; Jehng, J.-M.; Burcham, L. J.; Gao, X. *Catal. Today* **2000**, *57*, 323.
(4) *Catal. Today* **2000**, *57* (special issue devoted to group five compounds).
(5) *Catal. Today* **1996**, *28* (special issue devoted to niobium oxide compounds).
(6) *Catal. Today* **1993**, *16* (special issue devoted to niobium oxide compounds).
(7) *Catal. Today* **1990**, *8* (special issue devoted to niobium oxide compounds).
(8) Ushikubo, T.; Wada, K. *J. Catal.* **1994**, *148*, 138.
(9) Tanaka, T.; Nojima, H.; Yamamoto, T.; Takenaka, S.; Funabiki, T.; Yoshida, S. *Phys. Chem. Chem. Phys.* **1999**, *1*, 5235.
(10) Noureddini, H.; Kanabur, M. *JAOCS* **1999**, *76*, 305.
(11) Grenoble, D. C.; Murrell, L. L. U.S. Patent 4,415, 437, 1983.
(12) Wachs, I. E. U.S. Patent 4,544,649, 1985.
(13) Baltes, M.; Kytökivi, A.; Weckhuysen, B. M.; Schoonheydt, R. A.; Voort, P. V. D.; Vansant, E. F. *J. Phys. Chem. B* **2001**, *105*, 6211.
(14) Vuurman, M. A.; Wachs, I. E. *J. Mol. Catal.* **1992**, *77*, 29.
(15) Takenaka, S.; Tanaka, T.; Funabiki, T.; Yoshida, S. *J. Phys. Chem. B* **1998**, *102*, 2960.
(16) Niemantsverdriet, J. W. *Spectroscopy in Catalysis: An Introduction*; Wiley-VCH: Weinheim, 2000.
(17) González, J.; Del, M.; Ruiz, C.; Rivarola, J. B. *J. Mater. Sci.* **1998**, *33*, 4173.
(18) Stephenson, N. C.; Roth, R. S. 1. *J. Solid State Chem.* **1971**, *3*, 145; *Acta Crystallogr.* **1971**, *B27*, 1037.
(19) Tatibouët, J. M. *Appl. Catal. A* **1997**, *148*, 213.
(20) Hardcastle, F. D.; Wachs, I. E. *Solid State Ionics* **1991**, *45*, 201.
(21) Brown, I. D.; Wu, K. K. *Acta Crystallogr. B* **1976**, *32*, 1957.
(22) Deo, G.; Wachs, I. E. *J. Phys. Chem.* **1991**, *95*, 5889.
(23) Kosmulski, M. *Chemical Properties of Material Surfaces*; Marcel Dekker: New York, 2001.
(24) Baes, C. F., Jr.; Mesmer, R. E. *The Hydrolysis of Cations*; John Wiley & Sons: New York, 1976.
(25) Aveston, J.; Johnson, J. S. *Inorg. Chem.* **1964**, *3*, 1051.
(26) Gao, X.; Bare, S. R.; Weckhuysen, B. M.; Wachs, I. E. *J. Phys. Chem. B* **1998**, *102*, 10842.
(27) Deo, G.; Wachs, I. E. *J. Catal.* **1994**, *146*, 323.
(28) Badlani, M.; Wachs, I. E. *Catal. Lett* **2001**, *75*, 137.
(29) Wachs, I. E.; Chen, Y.; Jehng, J.-M.; Briand, L. E.; Tanaka, T. *Catal. Today* **2003**, *78*, 13.
(30) Brown, D.; Haught, H.; Zeton Altamira: Pittsburgh, PA, unpublished results.